Co_3O_4/TiO_2 hetero-structure for methyl orange dye degradation

Mahabubur Chowdhury, Sarah Kapinga, Franscious Cummings and Veruscha Fester

ABSTRACT

Advanced oxidation processes based on sulphate radical generated by peroxymonosulphate (PMS) activation is a promising area for environmental remediation. One of the biggest drawbacks of heterogeneous PMS activation is catalyst instability and metal ion leaching. In this study, a simple organic binder mediated route was explored to substitute Ti^{4+} ions into the Co_3O_4 host lattice structure to create a Co-O-Ti bond to minimise cobalt leaching during methyl orange degradation. The catalyst was characterised by X-ray diffraction, and scanning and transmission electron microscopy. The as-prepared catalysts with Co_3O_4:TiO_2 ratio of 70:30 exhibited minimal leaching (0.9 mg/L) compared to other ratios studied. However, the pristine Co_3O_4 exhibited highest catalytic activity (rate constant = 0.41 min^{-1}) and leaching (26.7 mg/L) compared to composite material (70:30 Co_3O_4:TiO_2). Interestingly, the morphology of the composite and leaching of Co^{2+} ions were found to be temperature dependent, as an optimum temperature ensured strong Co-O-Ti bond for prevention of Co^{2+} leaching. The classical quenching test was utilised to determine the presence and role of radical species on methyl orange degradation. The fabricated catalyst also exhibited good catalytic activity in degrading mixed dyes and good recyclability, making it a potential candidate for commercial application.

Key words | advanced oxidation processes (AOPs), Co_3O_4, heterogeneous reaction, leaching, PMS, TIO_2

Mahabubur Chowdhury (corresponding author)
Sarah Kapinga
Veruscha Fester
Flow Process and Rheology Centre,
Cape Peninsula University of Technology,
Cape Town 8000,
South Africa
E-mail: *chowdhurym@cput.ac.za*

Mahabubur Chowdhury
Sarah Kapinga
Department of Chemical Engineering,
Cape Peninsula University of Technology,
Cape Town 8000,
South Africa

Franscious Cummings
Electron Microscope Unit,
University of the Western Cape,
Bellville 7535,
South Africa

INTRODUCTION

The expansion of industries such as textiles, polycarbonates, nylon, cleansers, herbicides, resin paint, wood, paper and pulp, and pharmaceuticals has brought about significant water pollution issues due to the release of organic pollutants into the water body (Fleeger *et al.* 2003). A large portion of these organic toxins are carcinogenic; hence water treatment is of significant importance. Hydroxyl radical ($^{\bullet}OH$) based advanced oxidation processes have received much consideration due to their high efficiency compared to other chemical, physical and biological processes for the removal of recalcitrant and harmful organic contaminants (Wei *et al.* 2015). Recently sulphate based radicals ($SO4^{\bullet-}$) have been shown to be a promising alternative over hydroxyl radicals in light of the fact that $SO4^{\bullet-}$ has a higher reduction potential (2.5–3.1 V) compared to $^{\bullet}OH$ (1.8–2.7 V) (Yang *et al.* 2009). Sulphate radicals are generally generated by both homogeneous and heterogeneous activation of peroxymonosulphate (PMS). PMS activation via homogeneous routes is usually more efficient compared to heterogeneous catalysis (Miyamura *et al.* 2007). Various transition metals such as Co(II), Ru(III), Fe(II), Ce(III), Mn(II), Fe(III), and Ni(II) have been used to activate PMS for $SO4^{\bullet-}$ generation in homogeneous systems, with Co(II) the best activator for PMS (Anipsitakis & Dionysiou 2004). A Co^{2+} based PMS activation reaction follows the mechanism given in Equation (1) below (Chan & Chu 2009):

$$Co^{2+} + HSO_5^- \rightarrow Co^{3+} + SO_4^{\bullet-} + HO^- \quad (1)$$

It must be noted that Co^{2+} ions are toxic and hence Co^{2+} based heterogeneous catalysts, i.e. Co_3O_4, are of interest. Pristine Co_3O_4 and Co_3O_4 supported on various metal oxide supports have been studied as a heterogeneous catalyst for PMS activation for degradation of organic

doi: 10.2166/wst.2018.383

pollutants (Chen *et al.* 2008; Shukla *et al.* 2010a, 2010b; Zhang *et al.* 2010; Liang *et al.* 2012; Muhammad *et al.* 2012; Saputra *et al.* 2012; Saputra *et al.* 2013a; Chowdhury *et al.* 2015a). Incorporation of Co ions into the support structure to form a bond is the most important factor in Co^{2+} leaching during the PMS activation reaction (Yang *et al.* 2007; Zhu *et al.* 2013). Among various supports, titanium dioxide (TiO_2) exhibited stronger cobalt-support interaction (Yang *et al.* 2008). One-dimensional Co_3O_4 nanomaterials have attracted special interest due to their promising application in rechargeable lithium ion battery materials as anode material (Hui *et al.* 2008; Tan *et al.* 2016). With the surge in usage of mobile and handheld devices, large amounts of Co_3O_4 waste materials are to be produced in future. However, a wet impregnation method is mostly used in literature to synthesise TiO_2 supported Co_3O_4 material (Yang *et al.* 2007, 2008; Zhu *et al.* 2013). This technique might not be useful when utilising the waste Co_3O_4 from battery materials, to create TiO_2 supported Co_3O_4 material, for obvious reason.

In this study, we have used an organic binder mediated route to synthesise TiO_2/Co_3O_4 hetero-structure catalyst from separate Co_3O4 and TiO_2 material instead of the wet impregnation method. This will allow an application to be found for waste Co_3O_4 produced from battery materials in future.

EXPERIMENTAL METHOD

Chemicals and materials

PMS – commercially known as oxone – methyl orange (MO), absolute ethanol (C_2H_6O; EtOH), tert-butyl alcohol ($C_4H_{10}O$, TBA), urea (CH_4N_2O), maleic acid ($C_4H_4O_4$), cobalt chloride ($CoCl_2$) and TiO_2 (anatase) were purchased from Sigma Aldrich South Africa. All reagents were of analytical grade and used without further purification.

Synthesis of $Co(OH)_2$

Cobalt hydroxide $Co(OH)_2$ was synthesised using a previously reported method (Wang *et al.* 2009). In a typical synthesis procedure, 18 g of $CoCl_2.6H_2O$ was dissolved in 300 mL of deionised water by stirring at room temperature. In another beaker 0.09 g of urea was dissolved in 300 mL water. The urea solution was then added dropwise to the $CoCl_2$ solution while stirring. The mixed solution was moved into a Teflon-lined autoclave. The autoclave was kept at 105 °C for 6 h and afterwards was permitted to cool at room temperature. The resulting pink-coloured precipitates were separated by centrifuging, followed by washing with distilled water and absolute ethanol for several times, followed by drying in an oven at 60 °C for 24 h. The role of urea was to release OH^- ions at elevated temperature and pressure in the reactor, which reacts with Co^{2+} to precipitate $Co(OH)_2$. Decomposition of urea produces NH_3 and CO_2 followed by the release of OH^- (Ibupoto *et al.* 2014).

Synthesis of TiO_2/Co_3O_4 hetero-structure material

An organic linker mediated route was used to create a chemically bonded interface between TiO_2 and Co_3O_4. The method of synthesis was adopted from our previous studies (Oghenochuko *et al.* 2015; Chowdhury *et al.* 2015b, 2016). Seven different ratios (wt%) of Co_3O_4/TiO_2 composite, namely 98:2, 95:5, 90:10, 85:15, 80:20, 70:30 and 60:40, were prepared. In a typical synthesis $Co(OH)_2$ and TiO_2 (anatase) were independently suspended in 30 mL of ethanol (labelled as suspension A and B respectively); then 10 mL of 0.1 mol/L maleic acid was added to suspension A. The suspensions were stirred at room temperature for around 5 h. Suspension A was then added to suspension B and the mixture was stirred for 24 h at room temperature. The role of maleic acid was to anchor the TiO_2 on the $Co(OH)_2$ surface through its dicarboxylic functional group (Kim *et al.* 2009). The resulting catalyst was collected by centrifuging and washing with distilled water and absolute ethanol for a few times and dried in a vacuum oven at 60 °C overnight. After the anchoring process the dried powder was annealed at elevated temperature of 600 °C in air for 4 h. Catalytic activity data reported in this study were obtained from the catalyst synthesised at 600 °C unless otherwise stated.

Evaluation of catalytic activity

The system was made out of a 250 mL jacketed glass reactor containing 200 mL of MO (40 mg/L). A specific amount of Co_3O_4/TiO_2 catalyst was dispersed via sonication in the MO solution. The solution was left under stirring for 30 min to reach adsorption equilibrium. A certain amount of oxone was added to the solution. A 2 mL sample of the solution was regularly withdrawn from the reactor. The withdrawn sample was immediately diluted with equivalent volume of EtOH to quench ongoing catalytic reaction. Afterwards the collected sample was centrifuged to remove any solid catalyst. The concentration of MO without catalyst was analyzed by UV–Vis spectrophotometry (Shimadzu UV-2550) at the maximum absorption band (486 nm).

Characterisation

The crystal structures of the synthesised products were determined using X-ray diffraction (XRD); a Phillips PW 3830/40 Generator with Cu-Kα radiation was used. The structure of the catalysts was studied using a Tecnai $G^2$20 field emission gun transmission electron microscope (TEM) operated at 200 kV in bright-field mode. A Fischione high angular annular dark-field detector (HAADF) was used to collect dark-field scanning transmission electron microscopy (STEM) micrographs of the catalysts. A Gatan GIF-2001 electron energy spectrometer was used to collect electron energy loss spectroscopy (EELS) data, whereas all selected area electron diffraction (SAED) patterns were obtained by using a 200 nm diameter aperture. Energy dispersive X-ray spectroscopy data were collected in STEM mode, using an EDAX liquid nitrogen cooled Si(Li) detector.

RESULTS AND DISCUSSION

Structural evaluation of the catalyst

Temperatures of 350 and 600 °C were used to evaluate the role of temperature in the formation of Co_3O_4/TiO_2 composite material. Figure 1(a) shows the bright-field TEM image of the TiO_2/Co_3O_4 sample synthesised at 600 °C. Unlike the case when synthesised at 350 °C (Figure S1, supplementary information, available with the online version of this paper), the TiO_2 and Co_3O_4 do not exist as separate materials; instead, as shown, the nanostructures form rods of individual nanoparticles. It can be postulated that at higher temperature individual particles diffuse together to form rod-like structures. A graphical illustration of the rod-like structure formation is presented in the supplementary information (Figure S2, available online). The high-resolution micrograph of Figure 1(b) shows a uniform lattice fringe size (d-spacing) for the individual nanoparticles constituting the nanowires. The energy dispersive X-ray spectroscopy (EDS) spectrum of Figure 1(c), however, shows the elemental presence of Ti, Co and O in the nanowires, suggesting that at 600 °C the TiO_2 exists as a possible dopant in the Co_3O_4 matrix or forms a TiO_2/Co_3O_4 'alloy' or hybrid material. The SAED pattern of Figure 1(d) suggests the latter, as the diffraction pattern once more exhibits both the cubic crystal structure of Co_3O_4 and the tetragonal crystal phase of anatase TiO_2. From the analysis of this pattern, the lattice constant of Co_3O_4 matrix is determined as $a =$ 0.852 nm, with the lattice constants of the tetragonal TiO_2 determined as $a = 0.292$ nm and $c = 0.923$ nm. It was observed that there is an increase in the lattice constant of the cubic Co_3O_4 matrix synthesised at 600 °C compared to the case at 350 °C ($a = 0.820$ nm), accompanied by a decrease in the a and c axes (0.346 and 0.943 nm, respectively) of the tetragonal TiO_2 lattice. This implies that during the synthesis process at 600 °C, the TiO_2 lattice experiences a compressive stress in all three lattice axes, thereby inducing a smaller unit cell volume, which ultimately promotes the diffusion process.

HAADF-STEM coupled with EDS analysis was used to further confirm the inter-diffusion of TiO_2 and Co_3O_4 (Figure 2). The STEM-EDS spectral image of Figure 2(b) was collected from the boxed area indicated in Figure 2(a); the spectral image was collected using image pixels of 20×20 nm^2, each collected for 50 ms. Figure 2(d)–2(f) show the Ti, Co and O maps extracted from Figure 2(b). From these maps it becomes evident that the formation of hybrid TiO_2/Co_3O_4 is complete at 600 °C unlike catalyst synthesised at 350 °C (Figure S3, supplementary information, available online). XRD patterns of the pristine Co_3O_4, TiO_2 and TiO_2 supported Co_3O_4 prepared at 600 °C is presented in Figure S4 (supplementary information, available online). XRD patterns of the pristine Co_3O_4 and TiO_2 match the JCPDF card no: 42-1467 and 86-1156 respectively. Both pristine TiO_2 and Co_3O_4 peaks could be observed in the XRD patterns of the composite structure. This complements the observation from EDS and SAED as discussed above.

Figure 3 shows the EELS spectra of the Co_3O_4-TiO_2 structures annealed at 350 and 600 °C in comparison to that of pristine Co_3O_4 and TiO_2 at 350 °C. Figure 3(a) compares the energy loss near edge fine structure (ELNEFS) of the Co $L_{3,2}$ edges of a pristine Co_3O_4 specimen to that of the hybrid TiO_2/Co_3O_4 materials synthesised at 350 and 600 °C. The Co_3O_4 spectrum shows two sharp peaks at 789 eV (L_3) and 804 eV (L_2), which corresponds to the Co $2p_{3/2}$ and Co $2p_{1/2}$ spin–orbit peaks of the Co_3O_4 spinel structure (Hagelin-Weaver *et al.* 2004). The L_3/L_2 ratio is widely considered a fingerprint method for determining the Co valence state. From Figure 5(a) an L_3/L_2 ratio of 1.59, 1.46 and 1.49 is calculated for Co_3O_4, TiO_2/Co_3O_4 @350 °C and TiO_2/Co_3O_4 @600 °C, respectively. From these values it can be deduced that the pristine Co_3O_4 exists in the Co^{3+} oxidation state, typical of the Co_3O_4 electronic structure (Wang *et al.* 2000). Upon incorporation of the TiO_2 into the Co_3O_4 matrix it can be seen that the L_3/L_2 ratio decreases for the structures synthesised at both 350 °C and 600 °C.

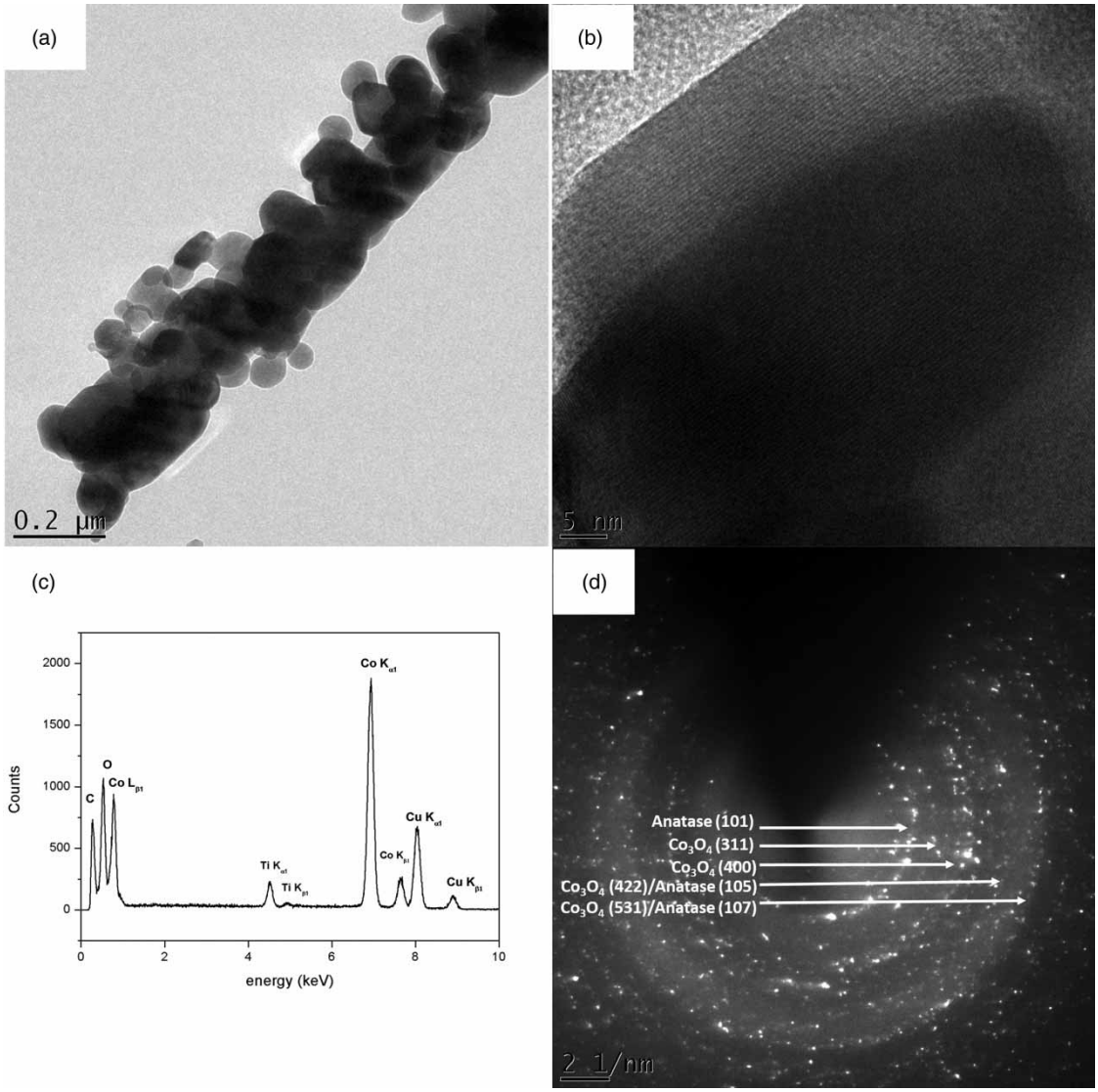

Figure 1 | (a) and (b) TEM bright field micrographs of sample, (c) EDS spectrum and (d) SAED pattern (sample prepared at 600 °C).

This suggest a re-coordination of the Co valency, caused by the TiO_2 diffusion into the Co_3O_4 matrix, resulting in the re-coordination of the Co valency due to the introduction of the Ti^{4+} ion. This successfully highlights the incorporation of TiO_2 into the Co_3O_4 lattice structure.

Figure 3(b) compares the ELNEFS of the Ti-$L_{3,2}$ edges of pure anatase TiO_2 to that of the TiO_2/Co_3O_4 synthesised at 350 and 600 °C. Unlike the case of the Co-$L_{3,2}$ ionisation edge, the L_3 and L_2 edges are separated by ~2.5 eV, with the L_2 edge more intense than L_3. At closer inspection it can be seen that both the L_2 and L_3 edges exhibit shoulders on the lower energy side of the peaks. This is typical of the anatase TiO_2 crystal structure caused by crystal-field splitting of the unoccupied, antibonding $t_{2\,g}$ and e_g orbitals which contain mostly titanium d character (Brydson *et al.* 1989). From these line shapes it becomes obvious that the TiO_2 structure undergoes no discernible change in lattice at either 350 or 600 °C and remains anatase. From the SAED results of Figure 1(d) it was shown that the TiO_2 unit cell volume decreases, which makes it favourable for diffusion into the Co_3O_4 lattice. The oxygen K edge at 532 eV exhibits three peaks at approximately 546, 552 and 566 eV. The first peak at 538–546 eV is indicative of lattice oxides (Abu-Zied *et al.* 2015) and hence the reshaping of this peak indicates a re-coordination in the lattice of the oxides. From Figure 3(b) it can be seen that the oxygen K edge becomes more pronounced at 600 °C due to the presence of the TiO_2 in the Co_3O_4 lattice, unlike the case at 350 °C. This confirms,

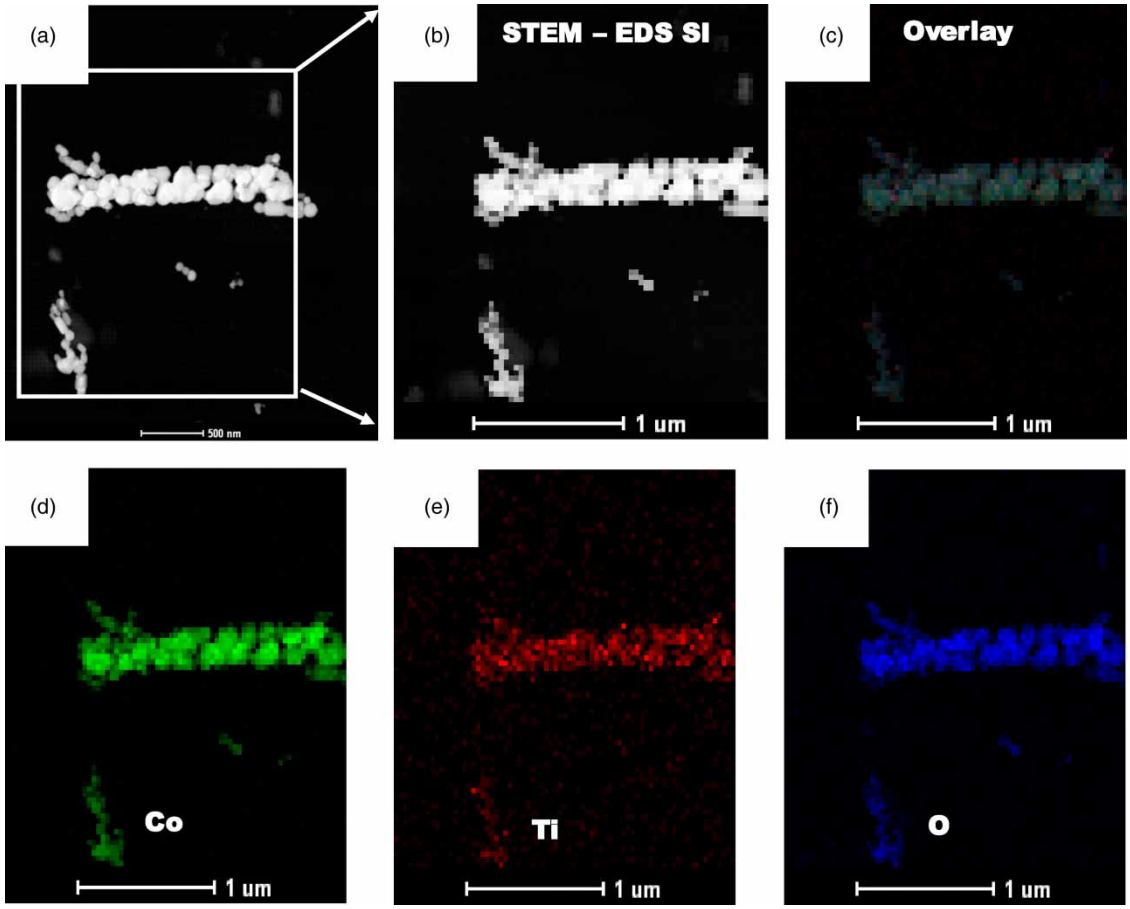

Figure 2 | (a) HAADF STEM micrograph of the composite Co_3O_4-TiO_2 material, (b) STEM-EDS spectral image of the area indicated in (a), (c) overlayed EDS map, (d)–(f) Co, Ti and oxygen maps extracted from the STEM-EDS spectral image of (b).

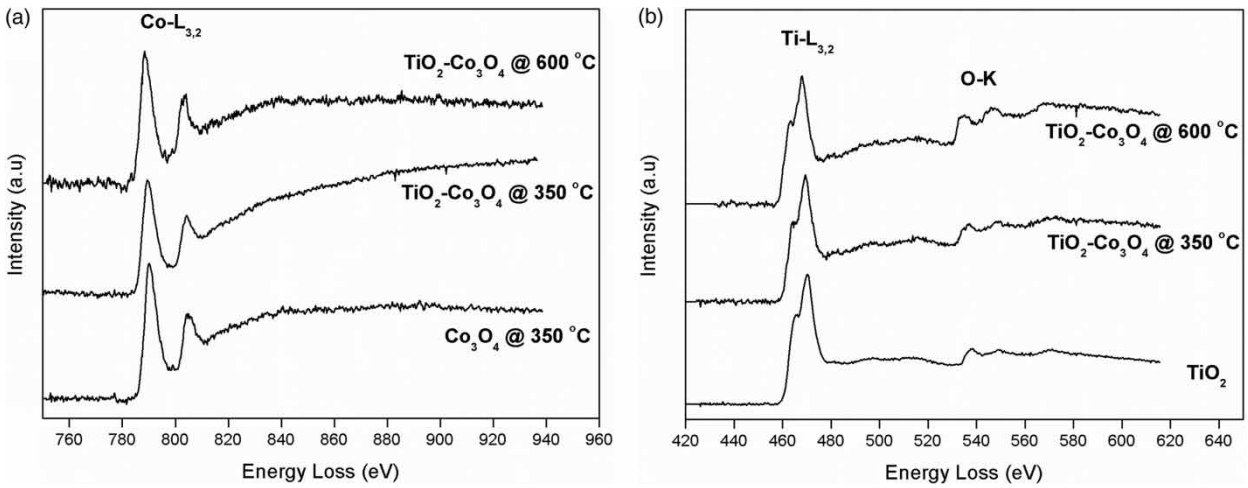

Figure 3 | Electron energy loss spectra comparing the energy loss near edge fine structures (ELNEFS) of the (a) Co-$L_{3,2}$ ionisation edge and (b) Ti-$L_{3,2}$ and O-K ionisation edges (ELNEFS) of the structures grown at 350 and 600 °C to that of pure Co_3O_4 and TiO_2 particles respectively.

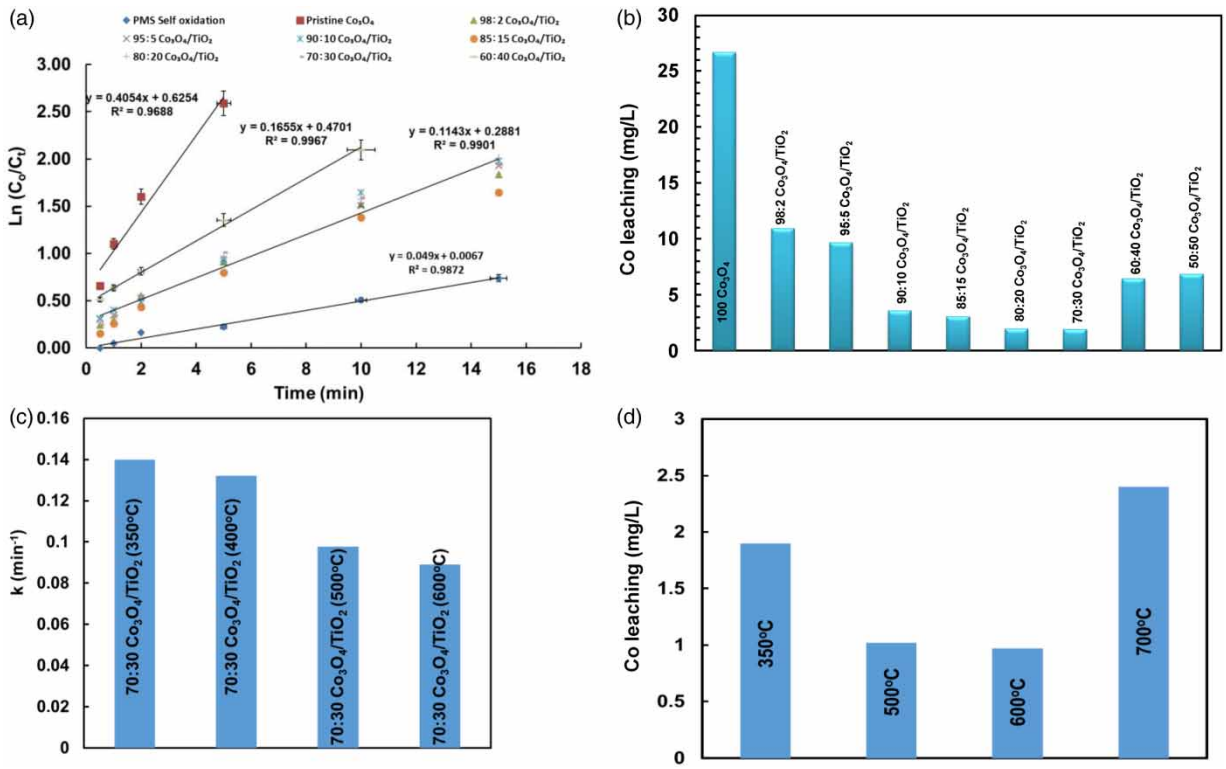

Figure 4 | Effect of Co_3O_4/TiO_2 ratio on (a) degradation kinetics of MO and (b) Co leaching; comparison of (c) degradation kinetics and (d) co-leaching for 70:30 Co_3O_4/TiO_2 catalyst synthesised at various temperatures (0.03 g/L catalyst load, 0.03 g/L oxone, 40 mg/L MO and 298 K)

once more, the analysis of the TEM and SAED results of Figures 1 and 2.

Catalytic activities and leaching of TiO_2 supported Co_3O_4 material

Figure 4(a) demonstrates the kinetic curves of heterogeneous PMS activation for the degradation of MO, while using pristine Co_3O_4 and various Co_3O_4 and TiO_2 ratios. Degradation of MO using PMS alone was also investigated to evaluate the role of PMS self-oxidation on the degradation of the dye. It can be seen that pristine Co_3O_4 exhibits the highest rate constant (k; 0.41 min^{-1}) while PMS on its own exhibits the lowest rate constant (k = 0.049 min^{-1}). It is interesting to note that the rate constant for the composite materials, in the range of 98:2 Co_3O_4/TiO_2 to 70:30 Co_3O_4/TiO_2 remains almost similar (k = ~0.11 min^{-1}), however lower compared to pristine Co_3O_4. This suggests that by introducing the TiO_2 as a support the quantity of Co_3O_4 utilised could be diminished (cobalt leaching is undesirable and Co^{2+} is toxic) while the catalytic activity could be maintained. Further reduction of Co_3O_4 amount in the Co_3O_4/TiO_2 composite material (60:40 Co_3O_4/TiO_2) resulted in higher catalytic activity (k = 0.17 min^{-1}) compared to other ratios studied in this study. Cobalt leaching is highlighted in Figure 4(b). It can be seen from Figure 4(b) that the cobalt leaching decreased with increasing TiO_2 amount in the composite material, up to a ratio of 70:30 Co_3O_4/TiO_2. A leaching amount of 1.9 and 26.7 mg/L was reported for 70:30 Co_3O_4/TiO_2 and pristine Co_3O_4. This highlights that by introducing TiO_2 as a support the amount of cobalt leaching can be reduced significantly. However, any further increase in TiO_2 amount in the composite structure increased the cobalt leaching. This is due to the fact that, when too much TiO_2 is used, a proper hetero-structure cannot form and leads to higher cobalt leaching. This results in a higher MO degradation rate constant as was observed in the case of 60:40 Co_3O_4/TiO_2 catalyst (Figure 4(b)). The 70:30 Co_3O_4/TiO_2 ratio was used as the optimum ratio as this catalyst exhibited minimum leaching. Removal of MO due to adsorption on the surface of Co_3O_4 and TiO_2 and interaction between TiO_2 and oxone was insignificant (Figure S5, supplementary information, available online; removal efficiency of MO in the presence of TiO_2 and oxone was lower than PMS self-oxidation). The effect of calcination temperature on the catalytic activity as well as on the cobalt leaching is shown in Figure 4(c) and 4(d). It can be seen that, with increasing calcination temperature catalytic activity decreases

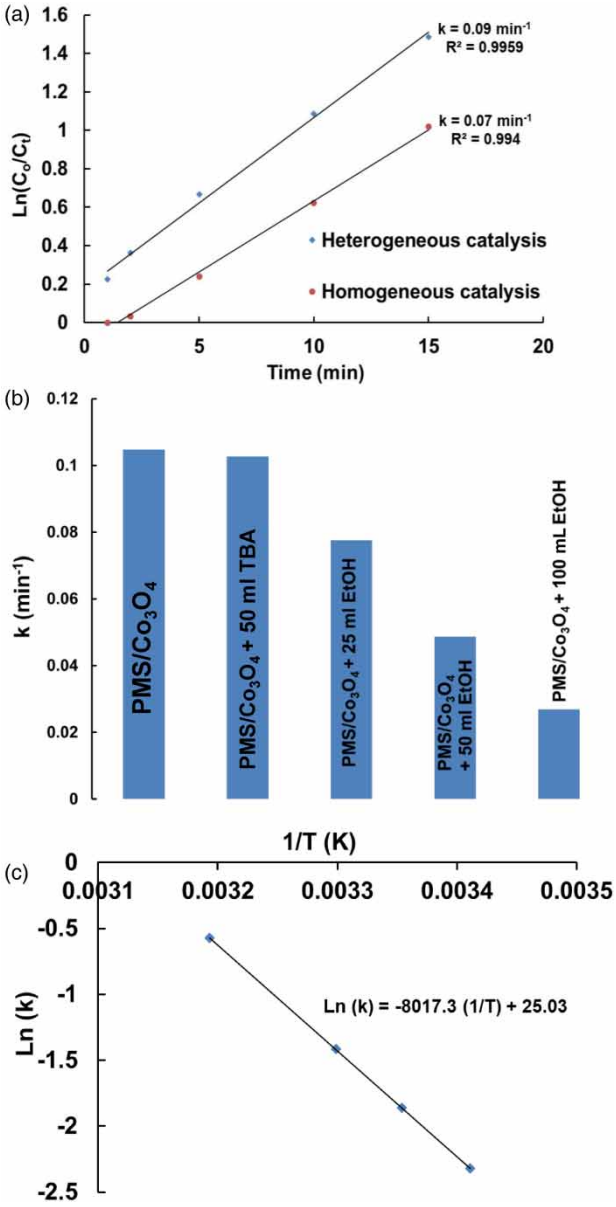

Figure 5 | (a) Comparison between homogeneous and heterogeneous PMS activation, (b) effect of quenching agent on MO degradation kinetic and (c) Arrhenius plot to determine the activation energy (0.03 g/L catalyst load, 0.03 g/L oxone, 40 mg/L MO and 298 K).

(Figure 4(c)), while the cobalt leaching first decreases with the increase of temperature (Figure 4(d)) in the range of 350–600 °C, but increases for catalyst calcined at 700 °C. This highlights a change in catalyst structure with temperature as was demonstrated earlier from the TEM analysis. Hence it can be postulated that there is a formation of a strong Co-O-Ti bond in the temperature range of 350–600 °C. This is due to the substitution of Ti^{4+} ions into Co_3O_4 host lattice as was previously confirmed from the ELNEFS study. Hence, a reduction of cobalt leaching was observed for that temperature range. However, cobalt oxide reduces to metallic cobalt at high temperature. It is well known that Co^0 can release Co^{2+} (Shi *et al.* 2015). Also, high calcination temperature might increase the Co_3O_4 grain size, thus reducing the contact area to the surface of the TiO_2 support. As a result, catalysts calcined at higher temperature are susceptible to leaching (Yang *et al.* 2009). Thus there was an increase of cobalt leaching when the catalyst was calcined at 700 °C. Catalyst (70:30 Co_3O_4/TiO_2) synthesised at 600 °C exhibited the lowest amount of leaching (0.9 mg/L) and was used further in this study unless otherwise stated.

Homogeneous experiments using dissolved cobalt concentrations (1.9 mg/L), higher than that leached (0.9 mg/L) from Co_3O_4/TiO_2 composite/hybrid, were performed to distinguish the role of homogeneous/heterogeneous catalysis in the degradation of MO. It can be seen from Figure 5(a) that the heterogeneous catalysis is more effective than the homogeneous catalysis. This implies that the Co_3O_4/TiO_2 catalyst calcined at 600 °C activated PMS via the heterogeneous route as a minimum of around 1 mg/L of dissolved Co is required to achieve the same extent of degradation via homogeneous PMS activation (Anipsitakis *et al.* 2006). The role of reactive species ($^{\bullet}OH$ and $SO_4^{\bullet-}$) in the degradation of MO was evaluated by a quenching test using EtOH and TBA as quenching agent. It has been established previously in literature that both $^{\bullet}OH$ and $SO_4^{\bullet-}$ could be generated from the PMS activation reaction (Anipsitakis & Dionysiou 2003; Saputra *et al.* 2013b). It can be seen from Figure 5(b) that in the presence of EtOH (various volumes added as can be seen from Figure 5(b)) notable decrease in reaction rate constant (k) occurred. Two different volumes of TBA (25 and 50 mL) were used to evaluate the role of $^{\bullet}OH$ in the MO degradation process. There was no significant decrease in rate constants in the presence of 25 and 50 mL TBA. However, a slight decrease in the reaction rate constant ($k = 0.08\ min^{-1}$) in the presence of 50 mL TBA compared to virgin solution ($k = 0.1\ min^{-1}$) was observed. This implies that $SO_4^{\bullet-}$ is the dominant reactive species that was generated by activating the PMS. The mechanism of PMS activation is given below (Wang *et al.* 2015):

$$Co^{2+} + HSO_5^- \rightarrow Co^{3+} + SO_4^{\bullet-} + HO^- \quad (2)$$

$$Co^{2+} + HSO_5^- \rightarrow Co^{3+} + SO_4^{2-} + {}^{\bullet}OH \quad (3)$$

$$^{\bullet}OH + SO_4^{\bullet-} + MO \rightarrow \text{several steps} \rightarrow CO_2 + H_2O + SO_4^{2-} \quad (4)$$

The effect of reaction temperature on the degradation kinetics of MO was investigated. Reaction rate constants increased significantly with increasing reaction temperature. Reaction rate constants of ~0.09, 0.16, 0.28 and 0.52 min^{-1} were obtained for temperatures of 20, 25, 30 and 40 °C respectively. This phenomenon is due to the rupture of the O-O bond and generation of $SO_4^{\bullet -}$ (Shi *et al.* 2012; Deng *et al.* 2017b). A higher reaction temperature also translates to a lower activation energy barrier. The activation energy (Ea), can be calculated with the classical Arrhenius equation as shown in Figure 5(c). The activation energy for 70:30 Co_3O_4/TiO_2 was found to be 66 kJ/mol. The Ea value is in the range (41–70 kJ/mol) of other reported Ea values for Co_3O_4 based systems (Saputra *et al.* 2013b; Deng *et al.* 2017a), and is higher than the activation energy required for diffusion-controlled reactions, which typically ranges from 10 to13 kJ/mol. This means that the MO removal was catalyst surface controlled.

Recyclability, effect of dye concentration and chemical oxygen demand removal efficiency of the catalyst

Recyclability or reusability of a heterogeneous catalyst is very important both from practical and economical points of view. It is always desirable to have a catalyst that can be reused without significant catalytic performance loss in industrial applications. The heterojunction catalyst was readily recycled just by centrifuging it from the solution and used in another batch for experiment without prior drying or calcination. The catalyst was recycled up to four times without any significant loss of catalytic activity as can be seen from Figure 6(a). In the first cycle 94% MO was removed after 30 min of reaction compared to 88% MO removal after 30 min in the fourth cycle. The effect of dye concentration on the catalytic activity of the catalyst was studied from 20 mg/L to 200 mg/L. It can be seen (Figure 6(b)) that the rate constant decreases with increases in initial dye concentration. Hence, it can be postulated that

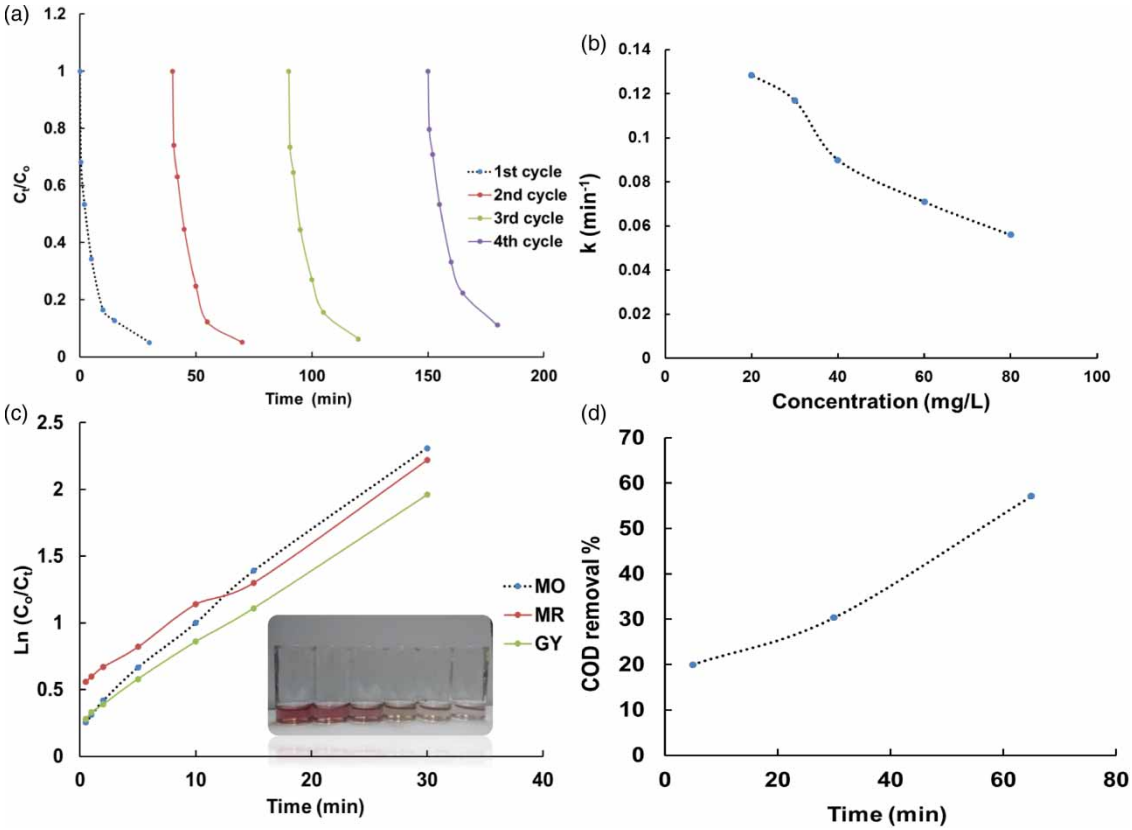

Figure 6 | (a) Recyclability of the as-prepared catalyst, (b) effect of initial dye concentration on MO degradation kinetics, (c) degradation kinetics of simulated dye bath water and (d) COD removal efficiency of the prepared catalyst.

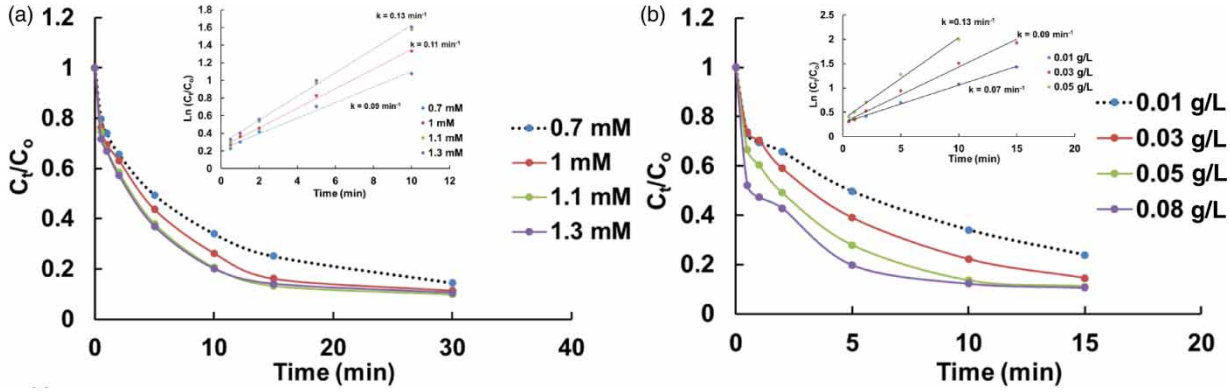

Figure 7 | Effect of PMS (a) and catalyst dosage (b) on the degradation of MO.

the dye concentration is a rate limiting step in the Co_3O_4/TiO_2-PMS oxidation reaction in this study. Synthetic dye bath effluent was prepared as an equal-amount mixture of three different dyes (60 mg/L total dye concentration), namely MO, golden yellow (GY) and methyl red (MR). This was done to evaluate the potential applications of the composite material in treating real industrial effluent. It can be seen from Figure 6(c) that the Co_3O_4/TiO_2 composite effectively decoloured the mixed dye. After 30 min of reaction a degradation of 95% was achieved for MO, 89% for MR and 86% for GY. Figure 6(c) shows the degradation kinetics of the mixed dye bath. Interestingly no significant difference in rate constants was observed for the three different dyes in the mixed bath. This implies that the catalyst has potential in degrading various dye types. The synthetic dye bath became colourless after 60 min of reaction (inset Figure 6(c)). From the environmental point of view, degradation of any organic pollutant, such as MO, is only the first step. It is well known that many intermediate compounds are formed during the degradation of MO. Chemical oxygen demand (COD) was measured to quantify the amount of organics present in the solution. It can be seen from Figure 6(d) that 57% of COD was removed after 60 minutes of catalytic reaction. This highlights the potential of the prepared material in practical wastewater treatment application.

Effect of PMS and catalyst dosage on MO degradation

Experiments were carried out to explore the effects of PMS and catalyst loading on the MO degradation in the oxidation of Co_3O_4/TiO_2. An increase in PMS loading from 0.7 to 1.1 mM and increase in catalyst loading from 0.01 to 0.05 g/L increased the MO degradation efficiency respectively (Figure 7(a) and 7(b)). However, a further increase in PMS and catalyst dosage to 1.3 mM and 0.08 g/L respectively did not enhance the MO degradation efficiency. When PMS and catalyst are present in excess dosage it might result in less availability of $SO_4^{\bullet-}$ due to the quenching mechanism. Huang and co-authors (Huang *et al.* 2014) showed, using EPR (electron paramagnetic resonance) technique, that when the PMS and catalyst are in excess it promotes the formation of nitroxide radicals and decreases the formation of $^{\bullet}OH$ and $SO4^{\bullet-}$ radicals. This results in lower degradation of the substrate.

CONCLUSION

This study investigated the heterogeneous PMS activation by TiO_2 supported Co_3O_4 catalyst. An organic binder mediated route was explored to create alloying/hybridisation between Co_3O_4 and TiO_2. Calcination temperature played an important role in controlling the catalyst morphology and Co-O-Ti bond. The pristine Co_3O_4 showed significantly higher removal efficiency of MO compared to TiO_2 supported Co_3O_4. However, TiO_2 supported Co_3O_4 resulted in significantly lower leaching than pristine Co_3O_4 material. This was due to the successful substitution of Ti^{4+} into the Co_3O_4 host lattice as was observed from the ELNEFS study, creating a strong Co-O-Ti bond. The 70:30 Co_3O_4/TiO_2 (calcined at 600 °C) exhibited the lowest amount of leaching. The as-prepared material also exhibited very good recyclability up to four cycles.

ACKNOWLEDGEMENTS

Mahabubur Chowdhury would like to thank the Cape Peninsula University of Technology for the research grant towards this project (URF 2017).

CONFLICTS OF INTEREST

The authors declare no conflicts of interest.

REFERENCES

Abu-Zied, B. M., Bawaked, S. M., Kosa, S. A. & Schwieger, W. 2015 Effect of microwave power on the thermal genesis of Co_3O_4 nanoparticles from cobalt oxalate micro-rods. *Applied Surface Science* **351**, 600–609.

Anipsitakis, G. P. & Dionysiou, D. D. 2003 Degradation of organic contaminants in water with sulfate radicals generated by the conjunction of peroxymonosulfate with cobalt. *Environmental Science & Technology* **37** (20), 4790–4797.

Anipsitakis, G. P. & Dionysiou, D. D. 2004 Radical generation by the interaction of transition metals with common oxidants. *Environmental Science & Technology* **38** (13), 3705–3712.

Anipsitakis, G. P., Dionysiou, D. D. & Gonzalez, M. A. 2006 Cobalt-mediated activation of peroxymonosulfate and sulfate radical attack on phenolic compounds. Implications of chloride ions. *Environmental Science & Technology* **40** (3), 1000–1007.

Brydson, R., Sauer, H., Engel, W., Thomass, J. M., Zeitler, E., Kosugi, N. & Kuroda, H. 1989 Electron energy loss and X-ray absorption spectroscopy of rutile and anatase: a test of structural sensitivity. *Journal of Physics: Condensed Matter* **1** (4), 797.

Chan, K. H. & Chu, W. 2009 Degradation of atrazine by cobalt-mediated activation of peroxymonosulfate: different cobalt counteranions in homogenous process and cobalt oxide catalysts in photolytic heterogeneous process. *Water Research* **43** (9), 2513–2521.

Chen, X., Chen, J., Qiao, X., Wang, D. & Cai, X. 2008 Performance of nano-Co_3O_4/peroxymonosulfate system: kinetics and mechanism study using Acid Orange 7 as a model compound. *Applied Catalysis B: Environmental* **80** (1–2), 116–121.

Chowdhury, M., Oputu, O., Kebede, M., Cummings, F., Cespedes, O., Maelsand, A. & Fester, V. 2015a Rapid and large-scale synthesis of Co_3O_4 octahedron particles with very high catalytic activity, good supercapacitance and unique magnetic properties. *RSC Advances* **5** (127), 104991–105002.

Chowdhury, M., Ntiribinyange, M., Nyamayaro, K. & Fester, V. 2015b Photocatalytic activities of ultra-small β-FeOOH and TiO_2 heterojunction structure under simulated solar irradiation. *Materials Research Bulletin* **68**, 133–141.

Chowdhury, M. R., Mpongwana, N., Cummings, F., Fester, V. & Ntwampe, S. 2016 β-FeOOH/TiO_2 Heterojunction for visible light driven photocatalytic inactivation of *E. coli*. In: *Photocatalysis* (W. Cao, ed.). Intech, The Netherlands.

Deng, J., Feng, S., Zhang, K., Li, J., Wang, H., Zhang, T. & Ma, X. 2017a Heterogeneous activation of peroxymonosulfate using ordered mesoporous Co_3O_4 for the degradation of chloramphenicol at neutral pH. *Chemical Engineering Journal* **308**, 505–515.

Deng, J., Ge, Y., Tan, C., Wang, H., Li, Q., Zhou, S. & Zhang, K. 2017b Degradation of ciprofloxacin using α-MnO_2 activated peroxymonosulfate process: effect of water constituents, degradation intermediates and toxicity evaluation. *Chemical Engineering Journal* **330**, 1390–1400.

Fleeger, J. W., Carman, K. R. & Nisbet, R. M. 2003 Indirect effects of contaminants in aquatic ecosystems. *Science of the Total Environment* **317** (1), 207–233.

Hagelin-Weaver, H. A. E., Hoflund, G. B., Minahan, D. M. & Salaita, G. N. 2004 Electron energy loss spectroscopic investigation of Co metal, CoO, and Co_3O_4 before and after Ar^+ bombardment. *Applied Surface Science* **235** (4), 420–448.

Huang, Z., Bao, H., Yao, Y., Lu, W. & Chen, W. 2014 Novel green activation processes and mechanism of peroxymonosulfate based on supported cobalt phthalocyanine catalyst. *Applied Catalysis B: Environmental* **154–155**, 36–43.

Hui, Z., Jianbo, W., Chuanxin, Z., Xiangyang, M., Ning, D., Jiangping, T. & Deren, Y. 2008 From cobalt nitrate carbonate hydroxide hydrate nanowires to porous Co_3O_4 nanorods for high performance lithium-ion battery electrodes. *Nanotechnology* **19** (3), 035711.

Ibupoto, Z. H., Elhag, S., AlSalhi, M. S., Nur, O. & Willander, M. 2014 Effect of urea on the morphology of Co_3O_4 nanostructures and their application for potentiometric glucose biosensor. *Electroanalysis* **26** (8), 1773–1781.

Kim, Y. J., Gao, B., Han, S. Y., Jung, M. H., Chakraborty, A. K., Ko, T., Lee, C. & Lee, W. I. 2009 Heterojunction of $FeTiO_3$ nanodisc and TiO_2 nanoparticle for a novel visible light photocatalyst. *Journal of Physical Chemistry C* **113** (5), 19179–19184.

Liang, H., Sun, H., Patel, A., Shukla, P., Zhu, Z. H. & Wang, S. 2012 Excellent performance of mesoporous Co_3O_4/MnO_2 nanoparticles in heterogeneous activation of peroxymonosulfate for phenol degradation in aqueous solutions. *Applied Catalysis B: Environmental* **127**, 330–335.

Miyamura, H., Matsubara, R., Miyazaki, Y. & Kobayashi, S. 2007 Aerobic oxidation of alcohols at room temperature and atmospheric conditions catalyzed by reusable gold nanoclusters stabilized by the benzene rings of polystyrene derivatives. *Angewandte Chemie* **119** (22), 4229–4232.

Muhammad, S., Saputra, E., Sun, H., Ang, H.-M., Tadé, M. O. & Wang, S. 2012 Heterogeneous catalytic oxidation of aqueous phenol on red mud-supported cobalt catalysts. *Industrial & Engineering Chemistry Research* **51** (47), 15351–15359.

Oghenochuko, O., Chowdhury, M., Nyamayaro, K. P. U. o., Cummings, F., Fester, V. & Fatoki, O. S. 2015 Novel β-FeOOH/NiO composite material as a potential catalyst for catalytic ozonation degradation of 4-chlorophenol. *RSC Advances* **5**, 59513–59521.

Saputra, E., Muhammad, S., Sun, H., Ang, H. M., Tadé, M. O. & Wang, S. 2012 Red mud and fly ash supported Co catalysts for phenol oxidation. *Catalysis Today* **190** (1), 68–72.

Saputra, E., Muhammad, S., Sun, H., Ang, H.-M., Tadé, M. O. & Wang, S. 2013a A comparative study of spinel structured Mn_3O_4, Co_3O_4 and Fe_3O_4 nanoparticles in catalytic oxidation of phenolic contaminants in aqueous solutions. *Journal of Colloid and Interface Science* **407**, 467–473.

Saputra, E., Muhammad, S., Sun, H., Ang, H.-M., Tadé, M. O. & Wang, S. 2013b Manganese oxides at different oxidation states for heterogeneous activation of peroxymonosulfate for phenol degradation in aqueous solutions. *Applied Catalysis B: Environmental* **142–143**, 729–735.

Shi, P., Su, R., Zhu, S., Zhu, M., Li, D. & Xu, S. 2012 Supported cobalt oxide on graphene oxide: highly efficient catalysts for the removal of Orange II from water. *Journal of Hazardous Materials* **229–230**, 331–339.

Shi, P., Wang, X., Zhou, X., Min, Y., Fan, J. & Yao, W. 2015 Influence of calcination temperature on the catalytic performance of Co_3O_4/GO nanocomposites for Orange II degradation. *RSC Advances* **5** (43), 34125–34133.

Shukla, P., Wang, S., Singh, K., Ang, H. M. & Tadé, M. O. 2010a Cobalt exchanged zeolites for heterogeneous catalytic oxidation of phenol in the presence of peroxymonosulphate. *Applied Catalysis B: Environmental* **99** (1–2), 163–169.

Shukla, P. R., Wang, S., Sun, H., Ang, H. M. & Tadé, M. 2010b Activated carbon supported cobalt catalysts for advanced oxidation of organic contaminants in aqueous solution. *Applied Catalysis B: Environmental* **100** (3–4), 529–534.

Tan, Y., Gao, Q., Li, Z., Tian, W., Qian, W., Yang, C. & Zhang, H. 2016 Unique 1D Co_3O_4 crystallized nanofibers with (220) oriented facets as high-performance lithium ion battery anode material. *Scientific Reports* **6**, 26460.

Wang, Z. L., Yin, J. S. & Jiang, Y. D. 2000 EELS analysis of cation valence states and oxygen vacancies in magnetic oxides. *Micron* **31** (5), 571–580.

Wang, G., Shen, X., Horvat, J., Wang, B., Liu, H., Wexler, D. & Yao, J. 2009 Hydrothermal synthesis and optical, magnetic, and supercapacitance properties of nanoporous cobalt oxide nanorods. *The Journal of Physical Chemistry C* **113** (11), 4357–4361.

Wang, Y., Zhou, L., Duan, X., Sun, H., Tin, E. L., Jin, W. & Wang, S. 2015 Photochemical degradation of phenol solutions on Co_3O_4 nanorods with sulfate radicals. *Catalysis Today* **258**, 576–584.

Wei, G., Liang, X., He, Z., Liao, Y., Xie, Z., Liu, P., Ji, S., He, H., Li, D. & Zhang, J. 2015 Heterogeneous activation of oxone by substituted magnetites $Fe_{3-x}M_xO_4$ (Cr, Mn, Co, Ni) for degradation of Acid Orange II at neutral pH. *Journal of Molecular Catalysis A: Chemical* **398** (Supplement C), 86–94.

Yang, Q., Choi, H. & Dionysiou, D. D. 2007 Nanocrystalline cobalt oxide immobilized on titanium dioxide nanoparticles for the heterogeneous activation of peroxymonosulfate. *Applied Catalysis B: Environmental* **74** (1–2), 170–178.

Yang, Q., Choi, H., Chen, Y. & Dionysiou, D. D. 2008 Heterogeneous activation of peroxymonosulfate by supported cobalt catalysts for the degradation of 2,4-dichlorophenol in water: the effect of support, cobalt precursor, and UV radiation. *Applied Catalysis B: Environmental* **77** (3), 300–307.

Yang, Q., Choi, H., Al-Abed, S. R. & Dionysiou, D. D. 2009 Iron–cobalt mixed oxide nanocatalysts: heterogeneous peroxymonosulfate activation, cobalt leaching, and ferromagnetic properties for environmental applications. *Applied Catalysis B: Environmental* **88** (3–4), 462–469.

Zhang, W., Tay, H. L., Lim, S. S., Wang, Y., Zhong, Z. & Xu, R. 2010 Supported cobalt oxide on MgO: highly efficient catalysts for degradation of organic dyes in dilute solutions. *Applied Catalysis B: Environmental* **95** (1–2), 93–99.

Zhu, Y., Chen, S., Quan, X. & Zhang, Y. 2013 Cobalt implanted TiO_2 nanocatalyst for heterogeneous activation of peroxymonosulfate. *RSC Advances* **3** (2), 520–525.

First received 27 April 2018; accepted in revised form 20 August 2018. Available online 30 August 2018